Applied Catalysis B: Environmental 108–109 (2011) 108–116

Contents lists available at SciVerse ScienceDirect

Applied Catalysis B: Environmental

journal homepage: www.elsevier.com/locate/apcatb

Comparative study of visible-light-driven photocatalytic mechanisms of dye decolorization and bacterial disinfection by B–Ni-codoped TiO_2 microspheres: The role of different reactive species

Wanjun Wang[a], Lizhi Zhang[b], Taicheng An[c], Guiying Li[c], Ho-Yin Yip[a], Po-Keung Wong[a,*]

[a] School of Life Sciences, The Chinese University of Hong Kong, Shatin, NT, Hong Kong, China
[b] Key Laboratory of Pesticide & Chemical Biology of Ministry of Education, College of Chemistry, Central China Normal University, Wuhan 430079, China
[c] State Key Laboratory of Organic Geochemistry, Guangzhou Institute of Geochemistry, Chinese Academy of Sciences, Guangzhou 510640, China

ARTICLE INFO

Article history:
Received 10 June 2011
Received in revised form 11 August 2011
Accepted 12 August 2011
Available online 19 August 2011

Keywords:
Photocatalysis
Dye decolorization
Bacterial disinfection
Partition system
Hydrogen peroxide

ABSTRACT

The controversy of mechanism still exists over whether photocatalytic decontamination proceeds via photon-generated h^+, e^-, $^\bullet OH$, $^\bullet O_2^-$ or H_2O_2. This study aims to investigate the roles of these reactive charges and oxidative species in the photocatalytic dye decolorization and bacterial disinfection processes in the presence of a visible-light-driven (VLD) photocatalyst, B–Ni-codoped TiO_2 microsphere, by employing various scavengers in the photocatalytic system and utilizing a novel partition system. Significant differences between VLD photocatalytic dye decolorization and bacterial disinfection are found. For photocatalytic dye decolorization, the reaction mainly occurs on the photocatalyst surface with the aid of surface-bounded reactive species (h^+, $^\bullet OH_s$ and $^\bullet O_2^-$), while bacterial cell can be inactivated by diffusing reactive oxidative species such as $^\bullet OH_b$ and H_2O_2 without the direct contact with the photocatalyst. The diffusing H_2O_2 plays the most important role in the photocatalytic disinfection, which can be produced both by the coupling of $^\bullet OH_b$ in bulk solution and $^\bullet OH_s$ on the surface of photocatalyst at the valence band. Furthermore, the $^\bullet O_2^-$, which is detected by using the electron spin resonance technique, is found to have direct function for the photocatalytic disinfection process. This study establishes a facile and versatile research methodology to investigate the VLD photocatalytic mechanism in different photocatalytic system.

1. Introduction

Semiconductor photocatalytic process has been widely applied as a "green" technology in treating environmental contaminants, such as the removal of the indoor organic pollutants and the decolorization and/or degradation of the soluble dyes in wastewater [1–3]. Since the pioneering work of bacterial disinfection in 1985 [4], inactivation of microorganisms through photocatalysis using titanium dioxide (TiO_2) irradiated by UV has also been extensively investigated [5–7]. To evaluate the efficiency of photocatalytic dye decolorization, we often monitor the concentration change of the organic dyes during photocatalytic reaction process, while for microbial inactivation, the cells will be attacked by photo-generated reactive species, leading to the damages of cell membrane, cell wall, and other intracellular components by oxidation. Unfortunately, most of these studies investigating the photocatalytic efficiency and mechanisms have only focused on either organic pollutants or microorganisms, and there is little information on the comparison between photocatalytic dye decolorization and bacterial disinfection [8].

The photocatalytic dye decolorization and bacterial disinfection share similar processes: (1) the semiconductor absorbs photons and generates electron–hole pairs; (2) the photoinduced electron–hole pairs are separated; (3) the oxidation of the organic compounds by the photo-generated holes (h^+) in the valence band (VB) or formed reactive oxygen species ($^\bullet OH$, $^\bullet O_2^-$, H_2O_2); (4) the reduction of oxygen by the photoelectron (e^-) in the conduction band (CB) [9,10]. The h^+, $^\bullet OH$, H_2O_2 and $^\bullet O_2^-$ are considered to be the major reactive species for the photocatalytic dye decolorization as well as bacterial disinfection [11]. However, which one of them plays the important role in the photocatalytic reaction process is still unclear, and quite different results are obtained in previous studies. For example, $^\bullet OH$ formed in the bulk solution ($^\bullet OH_b$) is more important for the degradation of 2,4-dichlorophenoxyacetic acid (2,4-D) in the presence of TiO_2 [12], while $^\bullet OH$ on the surface of photocatalyst ($^\bullet OH_s$) is responsible for the decomposition of 1,10-dichlorodecane (D_2C_{10}) [13]. In fact, the photocatalytic degradation rates under different conditions are significantly affected

* Corresponding author. Tel.: +852 2609 6383, fax: +852 2693 5767.
E-mail address: pkwong@cuhk.edu.hk (P.-K. Wong).

0926-3373/$ – see front matter © 2011 Elsevier B.V. All rights reserved.
doi:10.1016/j.apcatb.2011.08.015

by the adsorption amounts of organic pollutants onto TiO_2 surface [14]. In another study, direct h^+ oxidation pathway is dominated for the decolorization of methyl orange (MO) in the presence of photocatalyst, $Pb_2Sn_2O_6$ [15]. Another important issue is that whether the direct contact between the photocatalyst and organic pollutant/bacterial cell is required for the efficient photocatalytic oxidation process. Caballero et al. [16] has indicated that increasing the contact between the photocatalyst and bacterial cell enhances the disinfection process. However, MS-2 phage can also be inactivated mainly by the free •OH in the solution bulk (i.e. $•OH_b$) without direct contact with the photocatalyst [17]. The detail photocatalytic reaction processes and mechanisms for dye decolorization and bacterial disinfection is required a more systematical study.

Although TiO_2 has attracted much attention both in photocatalytic dye decolorization and bacterial disinfection, enhancing the TiO_2 photocatalytic activity under visible light or sun light is still a significant issue. Recently, we have synthesized a novel visible-light-driven (VLD) photocatalyst, B–Ni-codoped TiO_2 (BNT), via an aerosol-assisted flow method with hollow microspherical morphology [18]. The as-prepared sample exhibits superior photocatalytic activity for NO removal under visible light (VL) irradiation.

In the present work, the VLD photocatalytic application of BNT microspheres is further extended to both dye decolorization and bacterial disinfection in aqueous media. The roles of the major reactive (charged or oxidative) species are discussed based on the scavengers study. Moreover, a simple and novel partition system with a semi-permeable membrane is employed to separate photocatalyst from dye molecule/bacterial cell [19,20] and determine whether the direct contact between the photocatalyst and pollutant is a prerequisite for the decolorization of organic dye and the inactivation of bacterial cell. The differences in photocatalytic reaction behaviors between dye decolorization and bacterial disinfection are carefully compared and analyzed. The research methodology using scavengers and the partition system is expected to shed light on the understanding of the mechanism in other VLD photocatalytic system.

2. Experimental

2.1. Materials

The BNT microspheres were prepared by an aerosol-assisted flow method according to our previous study [18]. Rhodamine B (RhB), and 4-hydroxy-2,2,6,6-tetramethylpiperidinyloxy (TEMPOL) were obtained from Sigma Chemical Co. (USA). KI, $K_2Cr_2O_7$ (Cr(VI)), NaF, sodium oxalate and isopropanol were from Riedel-deHaën Chemical Co. (Germany). $FeSO_4$–EDTA (Fe(II)) was from Ajax Chemicals (Australia). All of the chemicals were of analytical reagent grade and isopropanol was of HPLC grade and dehydrated. The X-ray diffraction (XRD) patterns were recorded on a Bruker D8 Advance X-ray diffractometer with Cu Kα radiation (λ = 1.54178 Å) at a scan rate of 0.05° 2θ/s. The accelerating voltage and the applied current were 40 kV and 40 mA, respectively. Scanning electron microscopy (SEM, JSM-5600) was used to characterize the morphology of the obtained products.

2.2. Photocatalytic decolorization of RhB and disinfection of *E. coli* K-12

The photocatalytic decolorization of RhB and disinfection of *E. coli* K-12 were conducted using a 300 W Xenon lamp (Beijing Perfect Light Co. Ltd., Beijing) with a UV cutoff filter (λ < 400 nm) as light source. The VL intensity was measured by a light meter (LI-COR, USA) and was fixed at 193 mW/cm^2. The final photocatalyst concentration, RhB concentration and cell density were adjusted to 100 mg/L, 5 mg/L and about 2×10^5 cfu (colony forming unit)/mL, respectively. Before irradiation, the suspension was magnetically stirred in dark for 60 min to ensure the establishment of an adsorption/desorption equilibrium between the photocatalyst and RhB/bacterial cell. A partition system was used to separate dye molecule/bacterial cell from the BNT surface [19,20]. Fig. 1 shows the setup of the partition system for photocatalytic decolorization of RhB. For photocatalytic bacterial disinfection, the RhB solution in the inner compartment of the setup was replaced with a suspension of *E. coli* K-12 suspended in saline solution (0.9% NaCl). The detailed experimental procedure can be found in our previous reports [19,20]. All the above experiments were conducted in triplicates.

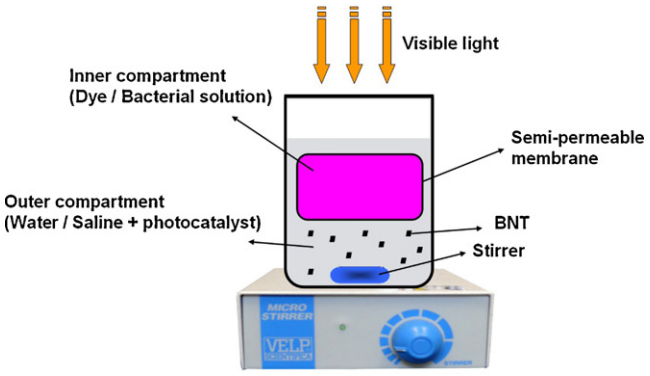

Fig. 1. Schematic illustration of partition system setup used in the photocatalyitc dye decolorization and bacterial disinfection by BNT under VL irradiation.

2.3. Analysis of reactive oxygen species

The formation of $•O_2^-$ and •OH were detected by electron spin resonance (ESR) technology. ESR signals of spin-trapped paramagnetic species with 5,5-dimethyl-1-pyrroline N-oxide (DMPO) were recorded with a Brucker A300 spectrometer. Also, the Xenon lamp with a UV cutoff filter (λ < 400 nm) was used as the light source. As $•O_2^-$ was very unstable in water and slow reaction with DMPO, the involvement of $•O_2^-$ was examined in methanol. The generation of •OH was also investigated through the method of photo-luminescence with terephthalic acid. The •OH was captured by terephthalic acid to produce a fluorescent product 2-hydroxyterephthalic acid [21,22], and then analyzed by a fluorescence spectrophotometer (Tecan, Männedorf, Switzerland, excitation wavelength: 315 nm; fluorescence peak: 425 nm).

Hydrogen peroxide (H_2O_2) was analyzed photometrically by the POD (horseradish peroxidase)-catalyzed oxidation product of DPD (N,N-diethyl-p-phenylenediamine) [23]. DPD readily reacted with H_2O_2 to produce the radical cation, $•DPD^+$, which was stabilized by resonance and formed a fairly stable color, with two absorption maxima at 510 nm and 551 nm (maximum wavelength). Fifty mg BNT was added into 50 mL of triple distilled water with VL irradiation. At different time intervals, aliquots of the sample were collected and analyzed at 551 nm by a UV-3600 (Shimadzu, Japan) spectrophotometer after the BNT being removed by centrifugation. For the surface analysis of F^- modified BNT, XPS experiments were performed on a Physical Electronics PHI 5600 multi-technique system, using monochromatized Al Kα radiation (1486.6 eV) at 350 W. All the binding energies were calibrated to the C 1 s peak at 284.8 eV of the surface adventitious carbon.

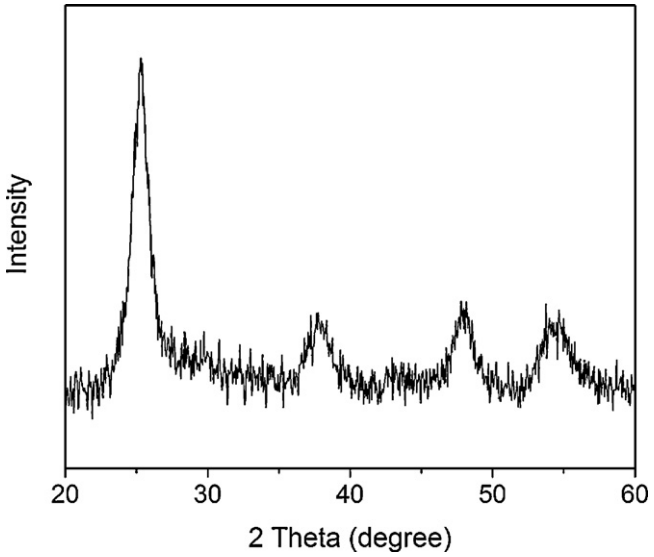

Fig. 2. XRD pattern of the B–Ni-codoped TiO_2 (BNT) products synthesized by the aerosol-assisted flow synthesis method.

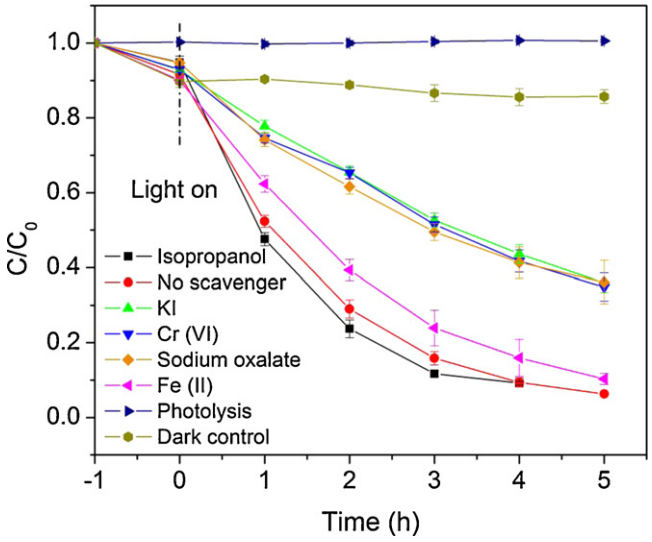

Fig. 4. Concentration changes of RhB (5 mg/L, 100 mL) at 553.5 nm as a function of irradiation time during the decolorization process in the presence of BNT (100 mg/L) with different scavengers (10 mmol/L isopropanol, sodium oxalate, KI, 0.5 mmol/L Cr(VI) and 0.1 mmol/L Fe(II)-EDTA) under VL irradiation (C_0, Original dye concentration before adsorption).

3. Results and discussion

3.1. XRD and SEM images

Fig. 2 shows the X-ray diffraction (XRD) pattern of the as-prepared BNT. All the peaks can be perfectly indexed as anatase phase of TiO_2 (JCPDS, file no. 84-1285). The average crystallite sizes calculated from the Scherrer equation is about 7.2 nm. Compared with that of undoped TiO_2, the crystalline size of TiO_2 increase after boron doping, while decrease with nickel doping. The typical SEM image of the as-prepared BNT is shown in Fig. 3. Hollow structured microspheres with 1–2 μm in diameter are clearly observed. The appearance of hollow structures could be ascribed to the escape of gas phase HBO_2 from the inner compartment of the TiO_2 microspheres during the pyrolysis reaction [18].

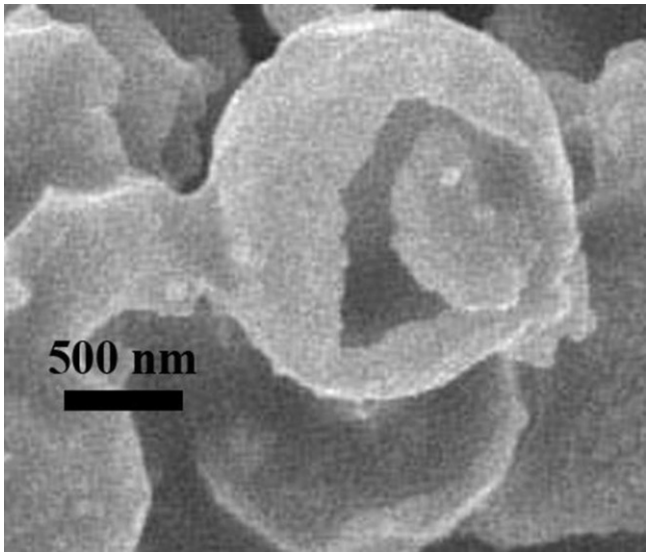

Fig. 3. Typical SEM image of the BNT synthesized with the aerosol-assisted flow synthesis method.

3.2. Photocatalytic decolorization of RhB

3.2.1. Role of reactive species

RhB is chosen as a representative synthetic dye to investigate the photocatalytic mechanisms for VLD photocatalytic dye decolorization by BNT. As mentioned above, the potential reactive species involved in the RhB decolorization process could be h^+, $^\bullet OH_b$, $^\bullet OH_s$, H_2O_2 and $^\bullet O_2^-$. In order to distinguish the role of these reactive species from each other, we perform the scavenger study, which employs different scavengers individually to remove the corresponding reactive species, so that we can understand the function of different reactive species in the photocatalytic RhB decolorization process based on the change of dye decolorization efficiency. The scavengers used in this study are sodium oxalate for h^+ [24], KI for h^+ and $^\bullet OH$ bound to the catalyst surface ($^\bullet OH_s$) [25], isopropanol for $^\bullet OH$ in the solution bulk ($^\bullet OH_b$) [25,26], Cr(VI) for e^- [25] and Fe(II) for H_2O_2 [20]. The initial pH value without scavengers is about 7.42. The pH value of the solution changes to 7.98, 7.22, 7.35, 7.38 and 6.58 after the addition of sodium oxalate, KI, isopropanol, Cr(VI) and Fe(II), respectively. Only slight decrease of photocatalytic efficiency is observed for dye decolorization and bacterial disinfection when the pH is changed from 6.5 to 7.95 (Fig. S2). Compared with the significant scavenging effect, the pH effect is much less important. In addition, Cho et al. has also reported that no significant pH effect, either on *E. coli* inactivation or on p-chlorobenzoic acid (pCBA) degradation, is observed when the pH is changed from 5.6 to 8.1 in the TiO_2-UV phtocatalytic system [27]. So the pH value influence on the photocatalytic activity with the addition of different scavengers can be negligible in this study. More than 98% of RhB can be decolored under VL irradiation within 5 h, indicating a good photocatalytic activity for the as-prepared BNT (Fig. 4). The reduction of total organic carbon (TOC) content reaches 77.9% after 5 h. To study the mechanism, isopropanol is usually used as a scavenger of $^\bullet OH_b$. The rate constant of reaction between $^\bullet OH_b$ and isopropanol is $1.9 \times 10^9\ M^{-1}s^{-1}$ [28], with a rate of almost the diffusion limit. Notably, with the addition of isopropanol to remove the $^\bullet OH_b$, the decolorization efficiency of RhB has no significant change, indicating that the $^\bullet OH_b$ is not a major reactive species (Fig. 4). However, in the presence of sodium oxalate and KI, the decolorization efficiency of RhB declines to only about 60% after

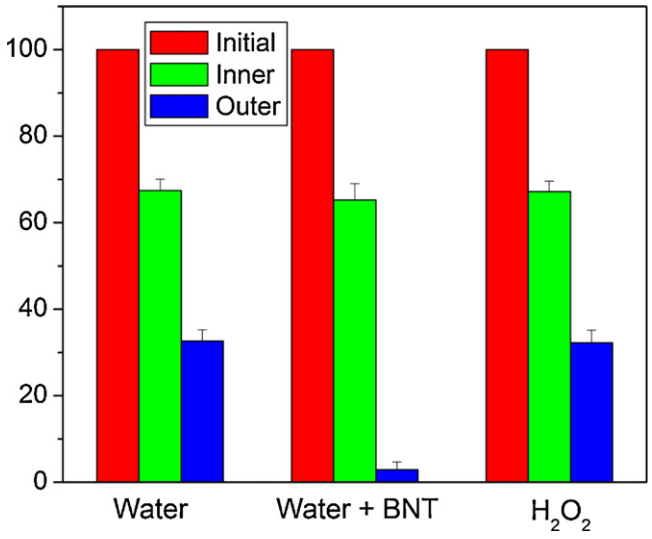

Fig. 5. Percentages of RhB (2.5 mg/L) in the inner and outer compartments of the partition system when the outer compartment is in various conditions (100 mg/L BNT, 0.1 mol/L H_2O_2) after 1 h VL irradiation.

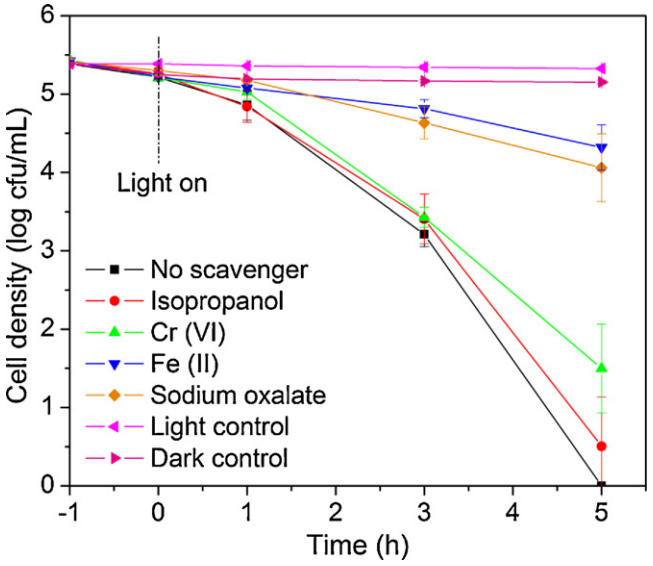

Fig. 6. Photocatalytic disinfection efficiency of *E. coli* K-12 by BNT under VL irradiation with different scavengers (0.05 mmol/L Cr(VI), 0.5 mmol/L isopropanol, 0.5 mmol/L sodium oxalate, 0.1 mmol/L Fe(II)-EDTA). BNT concentration = 100 mg/L, reaction volume = 50 mL, initial cell density = 2×10^5 cfu/mL.

5 h of irradiation. This indicates the h^+ or $^\bullet OH_s$ generated at the oxidation site of the photocatalyst plays an important role in VLD photocatalytic dye decolorization. The decrease of photocatalytic decolorization efficiency in the presence of Cr(VI) suggests $^\bullet O_2^-$ or $^\bullet OH_s$ generated at the reduction site of the photocatalyst is also involved in the decolorization process, since Cr(VI) can capture e^- which can then transform into $^\bullet O_2^-$ and $^\bullet OH_s$. The addition of Fe(II) (a H_2O_2 scavenger) has little influence on the decolorization efficiency indicates that H_2O_2 is not important in the photocatalytic decolorization process. To eliminate the possibility of RhB degraded by photo-sensitization, the experiment has also been conducted on VLD photocatalytic degradation of salicylic acid (SA) which cannot absorb visible light, and the similar results are obtained (Fig. S1). Thus, the major reactive species which are responsible for the VLD photoctalytic RhB decolorization can be h^+, $^\bullet OH_s$ and $^\bullet O_2^-$. Since h^+ and $^\bullet OH_s$ can only exist on photocatalyst surface, and $^\bullet O_2^-$ is not very stable in the solution [29], it may infer the photocatalytic decolorization of RhB occur only on the surface of photocatalyst.

3.2.2. Partition system for dye decolorization

To investigate the effect of direct contact between photocatalyst and RhB dye on the photocatalytic decolorization, we have developed a novel partition system to separate the BNT photocatalyst from the RhB molecules (Fig. 1). This partition system consists of a semi-permeable membrane with the molecular weight cutoff of 12,000–14,000 Da, which allows the free entry of small molecules such as water, H_2O_2, and all kinds of reactive oxygen species (ROSs) but only slow leakage of RhB. Fig. 5 shows the percentages of RhB in the inner and outer compartments of the partition system with different components in the outer compartment. When the outer compartment is water, about 64.4% RhB remains in the inner compartment after 1 h of VL irradiation. After adding the BNT in the outer compartment and irradiated by VL, the residual concentration of RhB in the inner compartment shows almost no difference as compared to that without addition of photocatalyst, indicating that no diffusing reactive species is involved in the decolorization process. H_2O_2 alone has no function for the dye decolorization either. These results suggest that for photocatalytic decolorization of RhB, the photoreaction mainly occurs on the photocatalyst surface with the oxidation of h^+, $^\bullet OH_s$ and $^\bullet O_2^-$.

3.3. Photocatalytic bacterial disinfection

3.3.1. Role of reactive species

E. coli K-12, the most commonly studied bacterium, is chosen as a model microbe to evaluate the inactivated performance and mechanism of BNT-VL system in photocatalytic bacterial disinfection. Without addition of scavenger, the bacterial cells can be completely inactivated within 5 h of VL irradiation, indicating a good photocatalytic disinfection activity of as-prepared BNT (Fig. 6). To study the photocatalytic mechanism, the scavengers for h^+ (sodium oxalate), e^- (Cr(VI)), $^\bullet OH_b$ (isopropanol), H_2O_2 (Fe(II)) are added individually during the disinfection process. Compared with dye decolorization, KI (a scavenger of h^+ and $^\bullet OH_s$) is too toxic for the bacterial cells and cannot be tested in the disinfection study (Fig. S3). Before conducting the experiment, the applied concentrations of each of the selected scavengers have been optimized to ensure their maximum scavenging effect but will not pose toxicity to the bacterial cells (Fig. S3). Oxalate is a good scavenger for h^+, however, the use of oxalate may produce $^\bullet CO_2^-$ [30], which may have toxic effect to the bacterial cells. To eliminate this potential problem, the experiments are conducted in the partition system under anaerobic condition. Argon (Ar) aeration together with oxalate addition does not cause any disinfection in the inner compartment of the partition system (Fig. S4), indicating that the possibly produced $^\bullet CO_2^-$ is not toxic or its life-span is too short to have function. In the presence of isopropanol, the photocatalytic disinfection efficiency is almost the same as that without scavenger addition, which indicates that $^\bullet OH_b$ is not involved in the inactivation process (Fig. 6). Meanwhile, with the addition of Cr(VI) to capture e^-, the disinfection efficiency is slightly decreased, indicating the photo-generated e^- is involved but may be not a major reactive species for photocatalytic disinfection. However, in the presence of sodium oxalate and Fe(II), the photocatalytic bacterial disinfection is greatly inhibited. Only about 1 log-reduction is achieved after 5 h of VL irradiation. As $^\bullet OH_s$ and H_2O_2 can be generated from h^+, the decrease of photocatalytic disinfection efficiency in the presence of sodium oxalate may be caused by the decrease of $^\bullet OH_s$ or H_2O_2 production. Based on the fact that Fe(II) alone has significant inhibition effect on disinfection efficiency, the H_2O_2 may play an important role in the VLD photocatalytic bacterial disinfection.

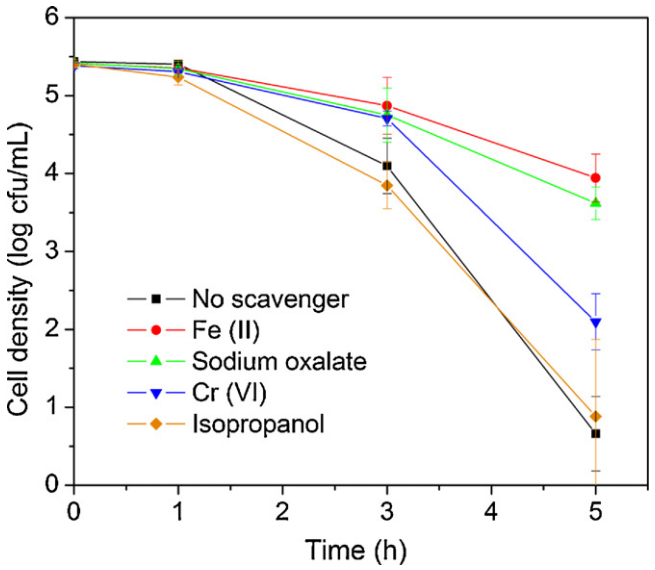

Fig. 7. Photocatalytic disinfection efficiency of *E. coli* K-12 (2×10^5 cfu/mL) in the inner compartment of the partition system. The outer compartment is the BNT suspension (100 mg/L) with different scavengers (0.05 mmol/L Cr (VI), 0.5 mmol/L isopropanol, 0.5 mmol/L sodium oxalate, 0.1 mmol/L Fe (II)-EDTA).

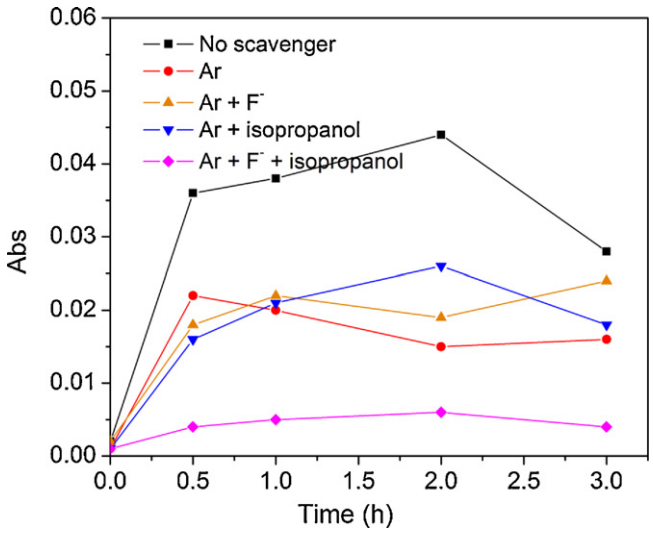

Fig. 8. Absorption intensity (551 nm) of the DPD/POD reagent after reacting with H_2O_2 produced in the presence of BNT (100 mg/L) with different modification conditions (5 mmol/L NaF, 0.5 mmol/L isopropanol) under different VL irradiation time (sampling volume = 2.7 mL).

3.3.2. *Partition system for bacterial disinfection*

To further confirm the role of H_2O_2 in the disinfection process, we also conducted the disinfection experiment using the partition system (Fig. 1). The bacterial cell suspension is added into the inner compartment, and BNT is added into the outer compartment. The cells of *E. coli* K-12 have molecular weight of about 2.6×10^6 Da, while the BNT microspheres have diameter of about 1–2 μm, so that both of them cannot pass through the membrane. Thus, the direct contact between bacterial cell and BNT is prohibited. A 5.3-log reduction of *E. coli* K-12 in the inner compartment is observed, when the BNT in the outer compartment is irradiated by VL for 5 h (Fig. S5). The disinfection efficiency is slightly lower as comparing to that in the non-partition system. It is probably due to the requirement of diffusion of reactive species ($^{\bullet}OH_b$ and H_2O_2) through the membrane to react with the bacterial cell in the inner compartment. In order to identify the diffusing reactive species, several scavengers are added into the outer compartment of the partition system to remove the respective reactive species. No disinfection is found in light and dark controls (Fig. S6). There is no obvious change of disinfection efficiency when isopropanol is added, indicating the $^{\bullet}OH_b$ is not important (Fig. 7). However, with the addition of Fe(II), the disinfection is significantly inhibited, which supports that the diffusing reactive species is H_2O_2, which can pass through the membrane to inactivate the bacterial cells. Meanwhile, Cr(VI) and sodium oxalate are also introduced into outer compartment of the partition system to block the H_2O_2 generation pathways from reduction and oxidation sites, respectively, since H_2O_2 can be produced by either e^- at reduction site or h^+ at oxidation site. Obviously, the results show that both Cr(VI) and sodium oxalate have inhibition effect on the disinfection efficiency, suggesting H_2O_2 coming from both reduction and oxidation sites. Compared with photocatalytic dye decolorization, which needs direct contact for the function, the photocatalytic bacterial disinfection can be achieved by the diffusing reactive species, H_2O_2, in the bulk solution without direct contact with photocatalyst.

It is found that the diffusing H_2O_2 play the most important role in the significant differences between VLD photocatalytic dye decolorization and bacterial disinfection. For dye decolorization the oxidative power of H_2O_2 is not enough to degrade organic dyes, such as RhB, which has complicated molecular structure. However, bacteria are procaryotic microorganisms that do not contain the nucleus characteristic of cells of higher plants and animals (eucaryotic cells). The DNA molecules do not have a nuclear membrane to separate them from the cytoplasm. Thus, the cytoplasmic membrane is extremely important in maintaining viability of cells. The electron carriers and enzymes responsible for the redox reactions must be properly linked on the membrane in order to couple the free energy change to ATP synthesis. Therefore, any disruption to the cell membrane integrity will cause the discharge of membrane potential and impose detrimental effects on cell survival [31]. The H_2O_2 can enter the cell and cause damage to the cell membrane, leading to the inactivation of the bacterial cells, although it may not degrade the organic components.

3.3.3. *Role of H_2O_2*

To detect the concentration of H_2O_2, we apply the DPD/POD method, which has been proved to be an effective method for low concentration of H_2O_2 [23]. Obviously, H_2O_2 is detected in this VLD photocatalytic system by using BNT as the photocatalyst (Fig. S7). The evolution of H_2O_2 as a function of irradiation time has also been monitored. Fig. 8 shows the absorption intensity (551 nm) of DPD/POD after reacting with H_2O_2 against illumination time under different modified conditions. It is found that the concentration of H_2O_2 quickly reaches a constant value after 1 h of irradiation, due to the decomposition of H_2O_2 in parallel with its production [32,33]. The equilibrium concentration for H_2O_2 is estimated to be 5.15 μmol/L. However, direct addition of this concentration of H_2O_2 does not have any bacterial disinfection effect (Fig. 9). It is suggested that, during the photocatalytic bacterial disinfection process, the H_2O_2 interacts with the bacterial cells in situ once it is produced. So the decomposition of H_2O_2 will be minimized, and the actual amount of H_2O_2 available to interact with the bacterial cell is much more than the amount detected. It is found that even the addition of 1 mmol/L H_2O_2 does not show strong bacterial disinfection ability. However, with the continuous addition of 1 mmol/L H_2O_2 every hour, the disinfection efficiency increases significantly. Also with the continuous addition of 5 μmol/L H_2O_2 every 3 min, bacterial disinfection is detected. These results indicate that small amount of H_2O_2 is produced and consumed continuously during the photocatalytic

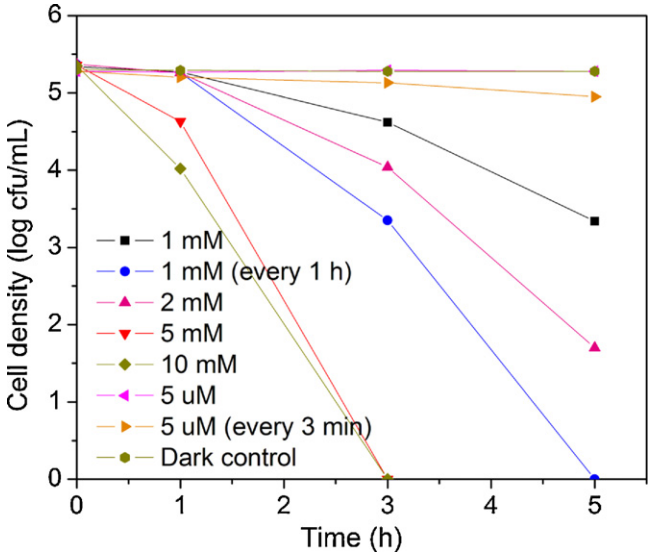

Fig. 9. Bacterial disinfection efficiency of *E. coli* K-12 (2×10^5 cfu/mL) by different concentration of H_2O_2.

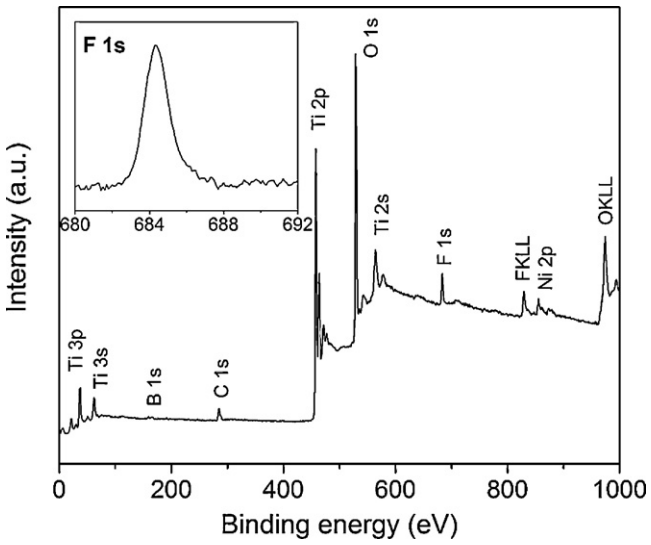

Fig. 10. XPS survey spectrum of F^- surface modified BNT powder. The inset is high resolution spectra of F 1s for the fluorinated BNT.

disinfection process. It is commonly accepted that H_2O_2 must be produced from conduction band by the following equations:

$$O_2 + e^- \rightarrow {}^\bullet O_2^- \quad (1)$$

$$H_2O + {}^\bullet O_2^- \rightarrow {}^\bullet OOH + OH^- \quad (2)$$

$$2{}^\bullet OOH \rightarrow O_2 + H_2O_2 \quad (3)$$

As mentioned above, the scavenger study in the partition system shows that H_2O_2 can also be generated from valence band without the participation of O_2. In fact, H_2O_2 can be formed by coupling of two $^\bullet OH$ in the bulk solution (Eqs. (4)–(7)):

$$h^+ + Ti^{IV}–O^{2-}–Ti^{IV}OH_2 \rightarrow \{Ti^{IV}–O^{2-}–Ti^{IV}\}–{}^\bullet OH_s + H^+ \quad (4)$$

$$h^+ + Ti^{IV}–O^{2-}–Ti^{IV}OH^- \rightarrow \{Ti^{IV}–O^{2-}–Ti^{IV}\}–{}^\bullet OH_s \quad (5)$$

$${}^\bullet OH_s \rightarrow {}^\bullet OH_b \quad (6)$$

$${}^\bullet OH_b + {}^\bullet OH_b \rightarrow H_2O_2 \quad (7)$$

When aeration of argon (Ar) removes O_2 in the solution and prevents any reactive species generated from conduction band, the production of H_2O_2 decreases (Fig. 8). Then, under the anaerobic condition, isopropanol is added to remove $^\bullet OH_b$. Interestingly, in the presence of $^\bullet OH_b$ scavenger, almost the same amount of H_2O_2 can also be detected, indicating that $^\bullet OH_s$ can directly form H_2O_2 on the photocatalyst surface.

To further investigate the role of $^\bullet OH_s$, we apply a F^- surface modified TiO_2 system to transform $^\bullet OH_s$ to $^\bullet OH_b$. Fluoride shows strong adsorption onto TiO_2 and the concentration of surface hydroxyl group (OH_s^-) on the photocatalyst can be controlled by adopting fluoride-exchange [34]. The process can be illustrated by the following equations [35]:

$$\equiv Ti^{IV}–OH + F^- \rightarrow \equiv Ti^{IV}–F + OH^- \quad (8)$$

$$\equiv Ti^{IV}–F + h^+ + H_2O/OH^- \rightarrow \equiv Ti^{IV}–F + {}^\bullet OH_b + H^+ \quad (9)$$

Recently, a significant enhancement of phenol degradation rate by photocatalytic oxidation in the presence of F^- has been reported and the enhancement is ascribed to the increased generation of $^\bullet OH_b$ [35,36], indicating the F^- modification is a practical way to significantly inhibit the formation of $^\bullet OH_s$ while increase the production of $^\bullet OH_b$. Fig. 10 shows XPS survey spectrum of F^- surface modified BNT powder that was prepared by adding NaF (5 mmol/L) in the aqueous BNT suspension (100 mg/L), filtering, and drying. The fluorinated sample clearly shows the peak of F 1 s as well as those of Ti, O, B and Ni elements. The C element is ascribed to the residual carbon from precursor solution and the adventitious hydrocarbon from the XPS instrument itself. The high resolution spectra of B 1s, Ti 2p, Ni 2p and their forms of chemical combination can be found in our previous report [18]. The F 1 s binding energy (BE) of 684.3 eV in this spectrum (inset of Figure 10) corresponds to that of F^- adsorbed on TiO_2, and no sign of F ions in the lattice (BE = 688.5 eV) is found [37,38], indicating that the F 1s peak is originated from the surface fluoride ($\equiv Ti^{IV}–F$) formed by ligand exchange between F^- and surface hydroxyl group on BNT [36]. It is found that the H_2O_2 production can also be observed with 5 mmol/L F^- modification (Fig. 8). It is because F^- surface modification will enhance the production of $^\bullet OH_b$, so that more H_2O_2 will be formed by coupling of $^\bullet OH_b$ in bulk solution [39,40]. However, in the presence of F^- and isopropanol, almost no H_2O_2 can be detected in the system.

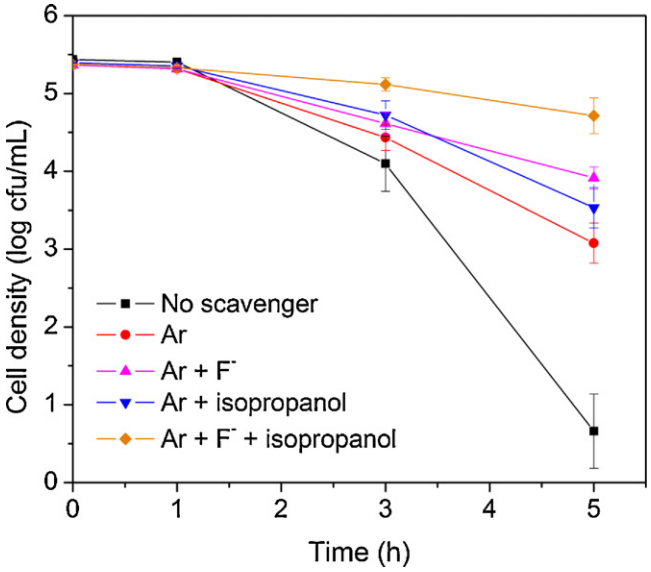

Fig. 11. Photocatalytic disinfection efficiency of *E. coli* K-12 (2×10^5 cfu/mL) in anaerobic condition (aeration of argon) in the inner compartment of the partition system. The outer compartment is the BNT suspension (100 mg/L) with different modification conditions (5 mmol/L NaF, 0.5 mmol/L isopropanol).

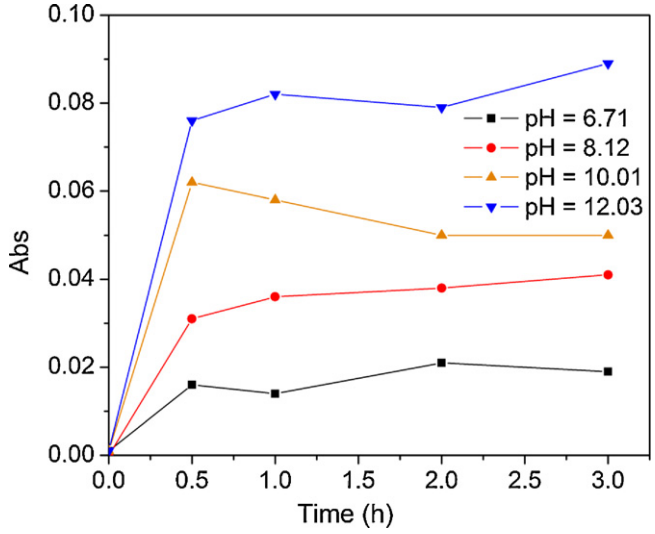

Fig. 12. Absorption intensity (551 nm) of the DPD/POD reagent after reacting with H_2O_2 produced in the presence of BNT (100 mg/L) under different pH value in anaerobic condition (aeration of argon) with VL irradiation (sampling volume = 2.7 mL).

These results provide the first experimental evidence that both $^{\bullet}OH_s$ and $^{\bullet}OH_b$ can combine to produce H_2O_2 at the valence band.

In order to further confirm the H_2O_2 production pathway from the valence band, the VLD photocatalytic bacterial disinfection in the partition system under anaerobic condition and the pH effect on the H_2O_2 production have been conducted. No disinfection occurs in dark and light controls in this experiment (Fig. S8). Under anaerobic condition with Ar aeration, neither F^- nor isopropanol can completely inhibit the photocatalytic bacterial disinfection efficiency in the partition system, unless both of them are added (Fig. 11). The disinfection efficiency is in proportion to the amount of H_2O_2 production (Fig. 8), which further supports that H_2O_2 is involved in the inactivation of bacterial cells. The amount of H_2O_2 produced from valence band at different pH has also been investigated under the anaerobic condition. It is found that more H_2O_2 will be generated if the pH is adjusted to a more alkaline value (Fig. 12), which can be explained by Eqs. (4)–(7). With the pH increasing, more $^{\bullet}OH$ will be produced, facilitating the evolution of H_2O_2 at the valence band. It is just the opposite with the reaction occurring at the conduction band, in which the H_2O_2 production will be inhibited with the increase of the pH [40].

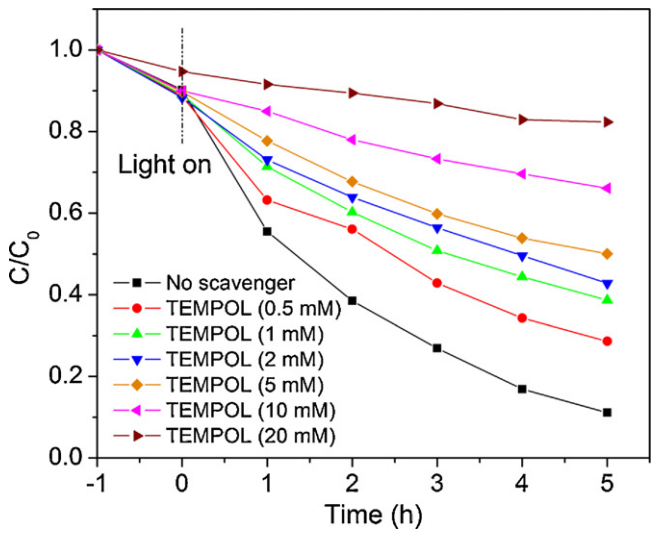

Fig. 13. Concentration changes of RhB (5 mg/L, 100 mL) at 553.5 nm as a function of irradiation time during the decolorization process in the presence of BNT (100 mg/L) with different concentration of TEMPOL under VL irradiation (C_0, original dye concentration before adsorption).

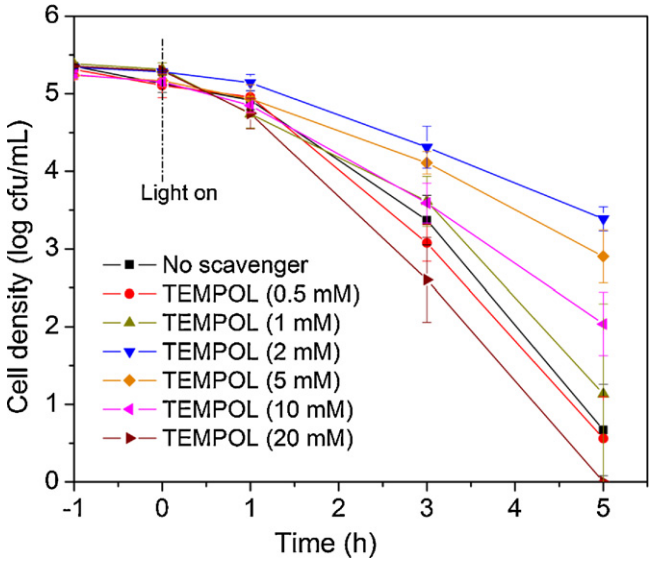

Fig. 14. Photocatalytic disinfection efficiency of *E. coli* K-12 by BNT with different concentration of TEMPOL under VL irradiation. BNT concentration = 100 mg/L, reaction volume = 50 mL, initial cell density = 2×10^5 cfu/mL.

3.4. Role of $^{\bullet}O_2^-$

To study the role of $^{\bullet}O_2^-$ in photocatalytic dye decolorization and bacterial disinfection process, we use 4-hydroxy-2,2,6,6-tetramethylpiperidinyloxy (TEMPOL), as the superoxide scavenger. TEMPOL is a water soluble analogue of the spin label TEMPO and is a stable piperidine nitroxide which can act as either an SOD mimetic or as a scavenger of superoxide anion [41]. No RhB decolorization and bacterial disinfection occur in dark and light controls (Figs. S9 and S10). Obviously, both the RhB decolorization and bacterial disinfection are greatly inhibited with the addition of TEMPOL (Figs. 13 and 14), which indicates that $^{\bullet}O_2^-$ is actually involved in

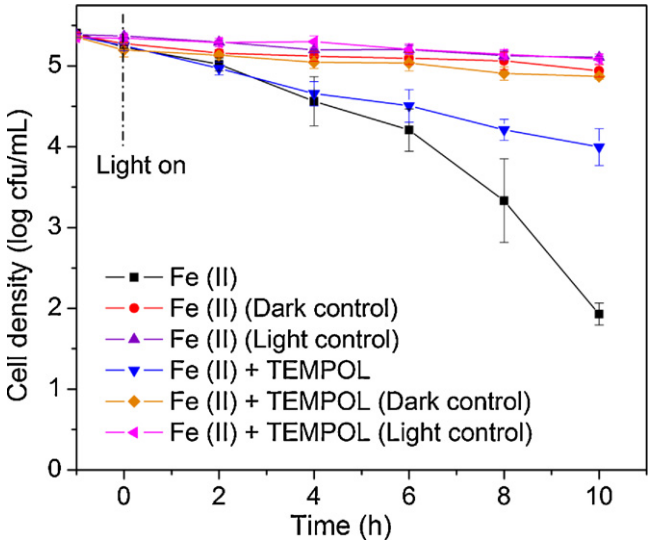

Fig. 15. Photocatalytic disinfection efficiency of *E. coli* K-12 by BNT under different scavenger conditions (0.1 mmol/L Fe(II)-EDTA, 2 mmol/L TEMPOL) with sequential addition. BNT concentration = 100 mg/L, reaction volume = 50 mL, initial cell density = 2×10^5 cfu/mL. The TEMPOL and a new batch of Fe(II) were added after 4 h of irradiation.

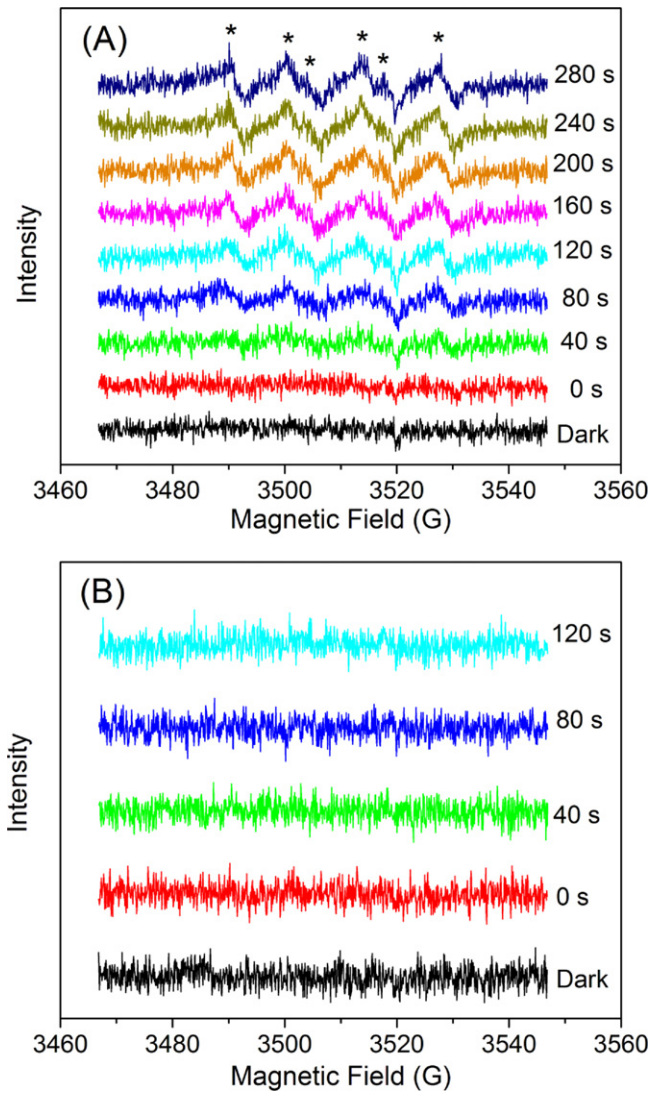

Fig. 16. DMPO spin-trapping ESR spectra recorded at ambient temperature in BNT suspension under VL irradiation ((λ > 400 nm). (A) For DMPO-•O_2^- in methanol dispersion, and (B) For DMPO-•OH in aqueous dispersion.

both processes. It is observed that when further increasing the TEMPOL concentration, the bacterial disinfection efficiency will first decrease followed by increase, while RhB decolorization efficiency is inhibited all the time. The increase of TEMPOL concentration will result in higher pH value (Table S1), which will in turn promote H_2O_2 production in the valence band, just as discussed above (Fig. 12). The promoted H_2O_2 can be used for increasing bacterial disinfection efficiency, but is not working for decolorization of dye.

The fact that no RhB decolorization occurs in the inner compartment of the partition system (Fig. 5) suggests that •O_2^- is not a diffusing radical, due to its extreme short life-span. It is only active on the surface of photocatalyst. However, the decrease of photocatalytic bacterial disinfection efficiency may be simply due to the decrease concentration of H_2O_2 which is highly responsible for the disinfection, as •O_2^- could produce H_2O_2 from the conduction band. To further confirm the role of •O_2^-, double scavengers study with a sequential addition is performed. First, Fe(II) is added to remove H_2O_2 and prevent the influence from H_2O_2. After 4 h of VL irradiation, TEMPOL is added to study the change of disinfection efficiency. To eliminate the possibility that Fe(II) may be insufficient to remove the continuously generated H_2O_2, a new batch of Fe(II) is also added in both cases of with and without TEMPOL addition. Results show that with the addition of TEMPOL in the presence of H_2O_2 scavenger, the disinfection is still inhibited, indicating the •O_2^- has direct function for the bacterial disinfection (Fig. 15). Importantly, this result provides the first experimental evidence that although •O_2^- is believed to be unstable and short life-span, it can directly involve in the bacterial disinfection rather than by producing other ROSs. Further study is being conducted to clarify its function.

In order to confirm the existence of •O_2^-, the ESR spin-trap with DMPO technique has also been carried out on illuminated BNT catalyst (Fig. 16(A)). In the dark, no signals can be detected. Under VL irradiation, the six characteristic peaks of the DMPO-•O_2^- adducts is observed, and their intensity increases with the irradiation time. This can double confirm that the formation of •O_2^- during the photocatalytic dye decolorization and bacterial disinfection processes in the presence of illuminated BNT photocatalyst. However, no characteristic peaks corresponding to DMPO-•OH is found when detecting the •OH production by ESR (Fig. 16(B)). Moreover, this result is further confirmed by fluorescence method using terephthalic acid as the •OH-trap agent (Fig. S11), further supporting the scavengers study that •OH in the bulk solution is not important in this VLD photocatalytic system, which may due to its extreme short life-span and quick combination to form H_2O_2.

4. Conclusions

In summary, we have revealed significant differences in the VLD photocatalytic mechanisms for dye decolorization and bacterial disinfection. For the RhB decolorization, the photo-reaction occurs mainly on the surface of the photocatalyst by the attacking of h^+, •OH_s and •O_2^-; while for bacterial disinfection, the bacteria can be inactivated in the bulk solution without direct contact with the photocatalyst. The diffusing H_2O_2 which can be generated form both conduction band and valence band plays the most important role in the photocatalytic bacterial disinfection. In the valence band, H_2O_2 is found to be produced both by the coupling of •OH_b in bulk solution and •OH_s on the surface of photocatalyst. Furthermore, the direct role of •O_2^- in photocatalytic decolorization and bacterial disinfection has also been confirmed by both scavengers addition experiments and ESR analysis. These findings provide foundation to design and fabricate facile VLD photocatalytic reactor for bacterial disinfection applications, since it does not need direct contact with the photocatalyst. Most importantly, this research methodology by utilizing various scavengers together with the partition system can be established as a versatile strategy to study the photocatalytic mechanism of different VLD photocatalytic system. Using this methodology to study different photocatalytic behaviors of other VLD photocatalysts is currently under investigation.

Acknowledgements

The project was supported by a research grant (GRF 477610) from the Research Grant Council, Hong Kong SAR Government, to P.K. Wong, NSFC (21073069 and 91023010) and Program for Innovation Team of Hubei Province (Grant 2009CDA048) to L.Z. Zhang and NSFC (21077104) to G.Y. Li and T.C. An. We would like to thank (1) State Key Laboratory Breeding Base of Photocatalysis, Fuzhou University and (2) Key Laboratory of Photochemistry, Institute of Chemistry, Chinese Academy of Sciences for conducting ESR analyses for this study.

Appendix A. Supplementary data

Supplementary data associated with this article can be found, in the online version, at doi:10.1016/j.apcatb.2011.08.015.

References

[1] M.R. Hoffmann, S.T. Martin, W.Y. Choi, D.W. Bahnemann, Chem. Rev. 95 (1995) 69–96.
[2] H. Lachheb, E. Puzenat, A. Houas, M. Ksibi, E. Elaloui, C. Guillard, J.M. Herrmann, Appl. Catal. B: Environ. 39 (2002) 75–90.
[3] C.E. Bonancêa, G.M. Nascimento, M.L. Souza, M.L.A. Temperini, P. Corio, Appl. Catal. B: Environ. 77 (2008) 339–345.
[4] T. Matsunaga, R. Tomoda, T. Nakajima, H. Wake, FEMS Microbiol. Lett. 29 (1985) 211–214.
[5] A.G. Rincón, C. Pulgarin, Appl. Catal. B: Environ. 49 (2004) 99–112.
[6] J. Lonnen, S. Kilvington, S.C. Kehoe, F. Al-Touati, K.G. McGuigan, Water Res. 39 (2005) 877–883.
[7] N. Baram, D. Starosvetsky, J. Starosvetsky, M. Epshtein, R. Armon, Y. Ein-Eli, Appl. Catal. B: Environ. 101 (2011) 212–219.
[8] F.N. Chen, X.D. Yang, F.F. Xu, Q. Wu, Y.P. Zhang, Environ. Sci. Technol. 43 (2009) 1180–1184.
[9] M.A. Fox, M.T. Dulay, Chem. Rev. 93 (1993) 341–357.
[10] J.W. Tang, Z.G. Zou, J.H. Ye, Angew. Chem. Int. Ed. 43 (2004) 4463–4466.
[11] J. Marugan, P. Christensen, T. Egerton, H. Purnama, Appl. Catal. B: Environ. 89 (2009) 273–283.
[12] J. Peller, O. Wiest, P.V. Kamat, J. Phys. Chem. A 108 (2004) 10925–10933.
[13] T.M. El-Morsi, W.R. Budakowski, A.S. Abd-El-Aziz, K.J. Friesen, Environ. Sci. Technol. 34 (2000) 1018–1022.
[14] H. Yang, G.Y. Li, T.C. An, Y.P. Gao, J.M. Fu, Catal. Today 153 (2000) 200–207.
[15] W. Wang, J. Bi, L. Wu, Z. Li, X. Wang, X. Fu, Nanotechnology 19 (2008) 505705.
[16] L. Caballero, K.A. Whitehead, N.S. Allen, J. Verran, J. Photochem. Photobiol. A 202 (2009) 92–98.
[17] M. Cho, H. Chung, W. Choi, J. Yoon, Appl. Environ. Microbiol. 71 (2005) 270–275.
[18] Y. Huang, W. Ho, Z. Ai, X. Song, L. Zhang, S. Lee, Appl. Catal. B: Environ. 89 (2009) 398–405.
[19] L.S. Zhang, K.H. Wong, D.Q. Zhang, C. Hu, J.C. Yu, C.Y. Chan, P.K. Wong, Environ. Sci. Technol. 43 (2009) 7883–7888.
[20] L.S. Zhang, K.H. Wong, H.Y. Yip, C. Hu, J.C. Yu, C.Y. Chan, P.K. Wong, Environ. Sci. Technol. 44 (2010) 1392–1398.
[21] H. Dong, Z. Li, X. Xu, Z. Ding, L. Wu, X. Wang, X. Fu, Appl. Catal. B: Environ. 89 (2009) 551–556.
[22] C. Li, F. Wang, J. Zhu, J.C. Yu, Appl. Catal. B: Environ. 100 (2010) 433–439.
[23] H. Bader, V. Sturzenegger, J. Hoigné, Water Res. 22 (1988) 1109–1115.
[24] R.C. Jin, W.L. Gao, J.X. Chen, H.S. Zeng, F.X. Zhang, Z.G. Liu, N.J. Guan, J. Photochem. Photobiol A 162 (2004) 585–590.
[25] Y.X. Chen, S.Y. Yang, K. Wang, L.P. Lou, J. Photochem. Photobiol A 172 (2005) 47–54.
[26] A.A. Khodja, A. Boulkamh, C. Richard, Appl. Catal. B: Environ. 59 (2005) 147–154.
[27] M. Cho, H. Chung, W. Choi, J. Yoon, Water Res. 38 (2004) 1069–1077.
[28] G.V. Buxton, C.L. Greenstock, W.P. Helman, A.B. Ross, W. Tsang, J. Phys. Chem. Ref. Data 17 (1988) 513–886.
[29] W. Ma, Y. Huang, J. Li, M. Chen, W. Song, J. Zhao, Chem. Commun. 158 (2003) 2–1583.
[30] F. Forouzan, T.C. Richards, A.J. Bard, J. Phys. Chem. 100 (1996) 18123–18127.
[31] G. Gottschalk, Biosynthesis of Escherichia coli cells from glucose, in: M.P. Starr (Ed.), Bacterial Metabolism, Springer-Verlag, New York, NY, 1979, pp. 34–80.
[32] Z. Zhang, X. Wang, J. Long, Z. Ding, X. Fu, X. Fu, Appl. Catal. A: Gen. 380 (2010) 178–184.
[33] F. Shiraishi, C. Kawanishi, J. Phys. Chem. A 108 (2004) 10491–10496.
[34] P. Calza, E. Pelizzetti, Pure Appl. Chem. 73 (2001) 1839–1848.
[35] C. Minero, G. Mariella, D. Maurino, V. Vione, E. Pelizzetti, Langmuir 16 (2000) 8964–8972.
[36] H. Park, W. Choi, J. Phys. Chem. B 108 (2004) 4086–4093.
[37] J.C. Yu, J. Yu, W. Ho, Z. Jiang, L. Zhang, Chem. Mater. 14 (2002) 3808–3816.
[38] Y. Huo, Y. Jin, J. Zhu, H. Li, Appl. Catal. B. Environ. 89 (2009) 543–550.
[39] K.T. Ranjit, I. Willner, S.H. Bossmann, A.M. Braun, Environ. Sci. Technol. 35 (2001) 1544–1549.
[40] Y. Kikuchi, K. Sunada, T. Iyoda, K. Hashimoto, A. Fujishima, J. Photochem. Photobiol. A 106 (1997) 51–56.
[41] D. Lejeune, M. Hasanuzzaman, A. Pitcock, J. Francis, I. Sehgal, Mol. Cancer 5 (2006) 21.